Heriot-Watt University
Research Gateway

Multichannel Metasurfaces for Anticounterfeiting

Citation for published version:
Zhang, C, Dong, F, Intaravanne, Y, Zang, X, Xu, L, Song, Z, Zheng, G, Wang, W, Chu, W & Chen, X 2019, 'Multichannel Metasurfaces for Anticounterfeiting', *Physical Review Applied*, vol. 12, no. 3, 034028. https://doi.org/10.1103/PhysRevApplied.12.034028

Digital Object Identifier (DOI):
10.1103/PhysRevApplied.12.034028

Link:
Link to publication record in Heriot-Watt Research Portal

Document Version:
Publisher's PDF, also known as Version of record

Published In:
Physical Review Applied

Publisher Rights Statement:
© 2019 American Physical Society

Phys. Rev. Applied 12, 034028

General rights
Copyright for the publications made accessible via Heriot-Watt Research Portal is retained by the author(s) and / or other copyright owners and it is a condition of accessing these publications that users recognise and abide by the legal requirements associated with these rights.

Take down policy
Heriot-Watt University has made every reasonable effort to ensure that the content in Heriot-Watt Research Portal complies with UK legislation. If you believe that the public display of this file breaches copyright please contact open.access@hw.ac.uk providing details, and we will remove access to the work immediately and investigate your claim.

Download date: 05. May. 2023

Multichannel Metasurfaces for Anticounterfeiting

Chunmei Zhang,[1] Fengliang Dong,[2,3] Yuttana Intaravanne,[1] Xiaofei Zang,[4] Lihua Xu,[2] Zhiwei Song,[2] Guoxing Zheng,[5] Wei Wang,[1] Weiguo Chu,[2,3,†] and Xianzhong Chen[1,*]

[1] *SUPA, Institute of Photonics and Quantum Sciences, School of Engineering and Physical Sciences, Heriot-Watt University, Edinburgh EH14 4AS, UK*

[2] *Nanofabrication Laboratory, CAS Key Laboratory of Nanosystem and Hierarchical Fabrication, CAS Center for Excellence in Nanoscience, National Center for Nanoscience and Technology, Beijing 100190, China*

[3] *Center of Materials Science and Optoelectronics Engineering, University of Chinese Academy of Sciences, Beijing 100049, China*

[4] *Shanghai Key Lab of Modern Optical System, University of Shanghai for Science and Technology, Shanghai 200093, China*

[5] *School of Electronic Information, Wuhan University, Wuhan 430072, China*

(Received 23 May 2019; revised manuscript received 2 August 2019; published 13 September 2019)

Anticounterfeiting is an effective method to decrease the harmful effects of counterfeit goods. Optical metasurfaces can tailor light's amplitude, phase, and polarization at subwavelength resolution, enabling compact optical devices with unusual functionalities that can outperform conventional bulky components. We propose and experimentally demonstrate a multichannel metasurface device that can reconstruct helicity multiplexed holographic images and hide a grayscale image in the polarization profile of a light beam, which can be used for high-level anticounterfeiting. A dielectric metasurface consisting of nanopillars with spatially variant orientations is used to realize distinct functionalities in multiple channels. The two holographic images can be switched by changing the helicity of the incident light, while the encoded image in the polarization profile of the light beam can be revealed by a polarizer. Our work demonstrates the feasibility of the multifunctional device based on the independent control of phase and polarization in different channels, which may open an alternative window for compact optical devices with high density of functionalities for anticounterfeiting.

DOI: 10.1103/PhysRevApplied.12.034028

I. INTRODUCTION

Driven by high profits, the potential harm and risks from the production and sale of fraudulent goods are big issues in our world. Much effort has been devoted to anticounterfeiting technologies. However, conventional methods for anticounterfeiting such as commonly used holograms are not very effective since they are outdated and easy to duplicate. Researchers have been looking for alternative holograms with unique properties that are not easy to design and are difficult to copy. Optical metasurfaces, two-dimensional counterparts of metamaterials, can tailor light's amplitude, phase, and polarization at subwavelength resolution, which can enable compact optical devices that possess unusual functionalities and can outperform conventional bulky components [1–3]. In the last several years, the broad appeal of this emerging technology has been focused on alternative discovery, performance improvement, device miniaturization, system integration, and alternative functionalities. Rapid advances in metasurfaces have brought about different design methodology, enabling the development of flat optics devices for various applications, ranging from metalenses [3–5], holograms [6–11], cloaking [12], and orbital angular momentum manipulation [13,14] to nonlinear optics [15].

To meet the growing requirement of device miniaturization and system integration, alternative design methodology based on metasurfaces has been proposed to develop ultrathin optical devices that integrate multiple functionalities into a single device while preserving their independent functionalities. The unprecedented capability of metasurfaces in light propagation provides a compact and flexible platform to realize various types of metasurface devices with multiple functionalities, including helicity multiplexed holograms [8], integration of multiple polarization manipulation channels [16], polarization beam splitters [17], and multifunctional light sword lenses [18]. As two fundamental properties of light, the spatial distribution of the polarization and phase can be used to record, process, and store information. For example, a high-resolution image can be encoded either

*x.chen@hw.ac.uk
†wgchu@nanoctr.cn

 © 2019 American Physical Society

in the phase profile [8] or in the polarization profile of a light beam [19,20]. A plethora of metasurface holograms [8,16,21–23] have been developed in the last several years. Notably, a twelve-polarization-channel hologram [16] and a vectorial hologram [24] have been recently developed. The former is realized by integrating multiple polarization manipulation channels for various spatial phase profiles into a single metasurface [16], while the latter is designed based on the linear relationship between phase and polarization modulations with displacements and orientations of identical meta-atoms [24]. How to realize a multichannel device that can realize an image-switchable hologram and nonuniform polarization profile for anticounterfeiting in different channels has not been reported. By integrating different functionalities (helicity multiplexed holograms and arbitrary polarization manipulation) onto the same metasurface device, a highly versatile ultracompact multichannel device with minimal spatial footprint can be achieved. Due to the independent control of phase and polarization based on the geometric phase, such a device is capable of realizing dynamic change of the holographic images and hiding a grayscale image. The encryption technique introduces hidden images for authentication, which can substantially increase the difficulty level of duplication and thus offer high-level security protection.

II. DESIGN AND METHODS

Figure 1 shows the schematic illustration of our proposed multichannel device, which combines the functionalities of a helicity multiplexed hologram and a spatially variant polarization profile onto a single metadevice. By controlling the helicity of the incident light, the device

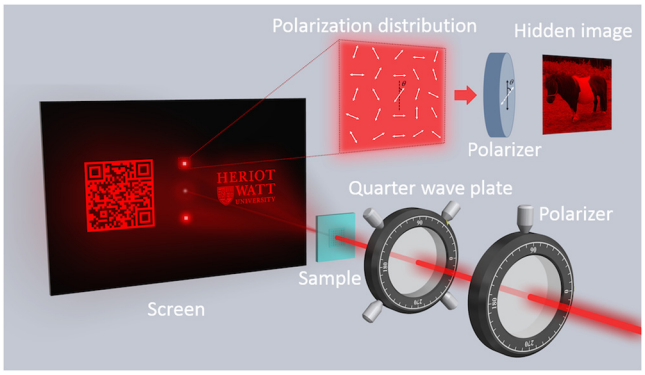

FIG. 1. Schematic of the multichannel metadevice for anticounterfeiting and encryption. A metasurface device can realize an image-switchable hologram and arbitrary polarization manipulation for hidden images. The two holographic images are switchable, depending on the helicity of the incident light, which is realized by a polarizer and a quarter wave plate. The polarization profiles of the laser beams along the vertical direction are used to hide a grayscale image, which can be revealed by passing through an analyzer.

can generate two holographic images [quick response (QR) code and logo of Heriot-Watt University] along two symmetrically distributed horizontal channels, which can be observed with naked eyes since the image size is proportional to the distance between the device and the screen. Upon the illumination of a linearly polarized light beam, the device can generate a nonuniform polarization profile along the vertical direction for encoding a grayscale image of a miniature horse. Although it can be revealed by using a rotating polarizer (analyzer), an objective lens is required to visualize the hidden image in detail due to the limited size of the device. Figure 2(a) shows the design parameters of the projected holographic images along the horizontal direction and the arbitrary polarization manipulation along the vertical direction. The full off-axis angles β_1, β_2, and β_3 are designed to be 65.7°, 19.0°, and 17.6°, respectively. The holographic images "QR code" and "University logo" have projection angles of 23.4° × 23.4° and 23.3° × 14.4°, respectively.

The Gerchberg-Saxton algorithm is used to calculate the phase profile of the hologram via a propagating function [25], which can reconstruct two off-axis images on the different sides of the incident light. The phase profile is precompensated in order to avoid image distortion because the final projected image has a large field of view of 65.7° × 23.4°. Details about the design and precompensation of the hologram are given in Refs. [7,8]. The target image includes a QR code and a University logo of Heriot-Watt University [see Fig. 2(b)]. Figure 2(c) shows the calculated phase distribution and the inset shows the phase distribution in the central area with a higher magnification.

To realize arbitrary polarization manipulation, a grayscale image (miniature horse) with 1125 × 1125 pixels is selected as a target image for polarization encoding [Fig. 2(d)]. Each pixel is 424 nm along two perpendicular directions. Malus' Law tells us that the intensity of the light transmitted by an analyzer is directly proportional to the square of the cosine of the angle between the transmission axes of the analyzer and the polarizer. In our experiment, the transmission axes of the polarizer and the analyzer are set along the x axis and y axis, respectively. The calculated polarization angle distribution of linearly polarized light is shown in Fig. 2(e). To realize off-axis configuration, an additional phase gradient profile is added. For this metasurface, the additional phase difference between neighboring pixels along the x direction is $\pi/5$, where the corresponding off-axis angle is 8.8°. Details of the off-axis design are provided in Sec. 1 of the Supplemental Material [26]. The required phase profile for the hologram and polarization profile for the hidden images are realized by controlling the orientation angles of nanopillars.

To realize different functionalities in multiple channels, metasurfaces for pure phase control [8] or simultaneous control of phase and polarization [16,17] are employed. In comparison with phase control, simultaneous control of

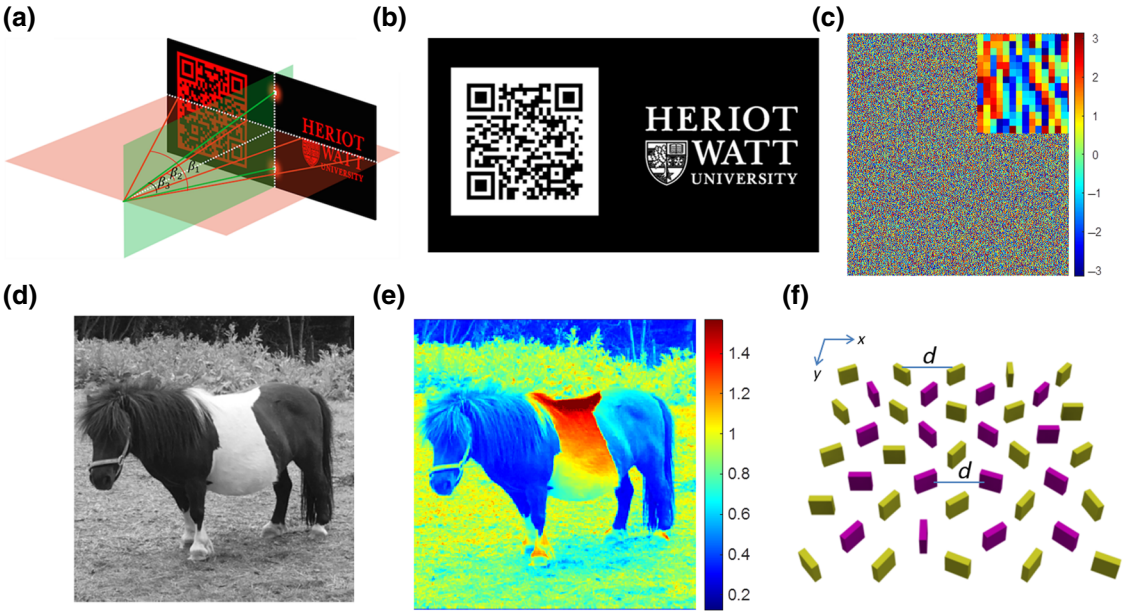

FIG. 2. Design and simulation. (a) Geometric parameters of the projected images and the off-axis vector beams for image encryption. The full off-axis angles β_1, β_2, and β_3 are designed to be 65.7°, 19.0°, and 17.6°, respectively. (b) The target holographic image and (c) the calculated phase profile based on the Gerchberg-Saxton algorithm. The inset in (c) shows the phase distribution in the central area with high magnification. There are 16 phase levels ($-\pi$ to π with the interval of $\pi/8$) that are used in the design. (d) The target object for image encryption and (e) the required distribution of polarization direction (in the unit of radians) for the linearly polarized light. (f) Two metasurfaces represented by gold and purple colors are merged together with a displacement vector of ($d/2$, $d/2$). d is the distance between neighboring antennas with a value of 424 nm. The size of the sample is the same and the equivalent pixel size is 300×300 nm^2 after the two metasurfaces are combined.

phase and polarization is more challenging for nanofabrication due to the precise control of the feature size. Instead of using dielectric nanopillars with various feature sizes, a metasurface consisting of nanopillars with the same feature size (e.g., height, length, width) and spatially variant orientations is used to facilitate the fabrication process. Two metasurfaces (one for the holographic image along the horizontal direction and one for arbitrary polarization manipulation along the vertical direction) are designed and merged together with a displacement vector of ($d/2$, $d/2$), as detailed in Fig. 2(f). The distance between neighboring nanopillars is d with a value of 424 nm along both the x and y directions. The nanopillars for two metasurfaces (represented by gold and purple colors) are arranged like a checkerboard. Suppose and $\theta_2(x,y)$ represent the calculated rotation angle distributions for the two separate metasurfaces, respectively. $\theta(x,y)$ represents the final rotation angle distribution for the nanopillars of the merged metasurface. The arrangement strategy can be expressed as

$$\theta(x,y) = \begin{bmatrix} \theta_1(x,y), & x = 2n,\ y = 2m-1 \text{ or } x = 2n-1,\ y = 2m \\ \theta_2(x,y), & x = 2n-1,\ y = 2m-1 \text{ or } x = 2n,\ y = 2m \end{bmatrix}, \tag{1}$$

where n and m are integer numbers ranging from 1 to 1125.

Each pixel of the dielectric metasurface functions as a half wave plate, which can generate the required independent phase profile for the designed hologram and the polarization profile for the hidden image based on Malus' Law. The sample size before and after metasurface merging is the same and the equivalent pixel size in the merged metasurface is 300×300 nm^2. The resonant wavelength of each nanopillar is dependent on its feature sizes, such as length (L_x) and width (L_y), which are used for efficiency optimization. The thickness h of the metasurface is 310 nm along the z direction. By rotating the fast axes of half wave plates with their orientations according to a function $\theta(x, y)$, a circularly polarized light beam can be fully transformed to a beam with opposite helicity and a geometric phase (known as a Pancharatnam–Berry phase) equal to $\pm 2\varphi(x, y)$. "+" and "−" represent the signs of the phase changes for the incident right-circularly polarized (RCP) light and for the incident left-circularly polarized (LCP) light, respectively. The reversion of the phase profile can be achieved by changing the helicity of the circularly polarized light. By controlling the local orientations of nanopillars between 0 and π, a phase profile that can cover the full 0–2π range while maintaining the equal transmission amplitude pickups can be achieved.

The designed silicon nanopillars are fabricated on quartz substrates. First, a 310-nm-thick film of amorphous silicon

is deposited on the substrate by using an Inductively Coupled Plasma Enhanced Chemical Vapor Deposition System (ICPECVD, Sentech SI 500D). Then a sputtering system (KJLC LAB18) is used to deposit an aluminum film with a thickness of 50 nm, which functions as a charge-dissipation layer and hard mask for etching. The positive electron beam resist (ZEP-520A) with a thickness of 200 nm is spin coated on the sample. After that, nanostructures are patterned on the resist film based on the standard electron-beam lithography (EBL, Vistec EBPG 5000+). The nanopatterns are transferred into the aluminum layer and silicon layer by subsequent etching using an Inductively Coupled Plasma etcher (ICP, Sentech PTSA SI 500). Finally, the silicon nanopillars are obtained by removing the residual aluminum with aluminum etchant.

III. RESULTS

The scanning electron microscope (SEM) image of part of the fabricated sample is shown in Fig. 3(a). The magnified SEM image for the sample with a tilt angle is shown in the inset of this figure. Figure 3(b) shows the schematic of the experimental setup to characterize the metasurface hologram. A tunable supercontinuum laser source (NKT-SuperK EXTREME) provides a laser beam with a wavelength of 650 nm, whose polarization state is controlled by a polarizer and a quarter wave plate (QWP). The laser beam impinges on the metasurface device, which is mounted on a three-dimensional (3D) translational stage, allowing for the adjustment of sample position. The transmitted holographic images are projected to a screen in the far field for inspection of the image quality. A normal camera is used to capture images on the image screen. Upon the illumination of LCP light, the fabricated device can reconstruct the "QR code" on the left and the "University logo" on the right side of the metasurface, respectively [Fig. 3(c)]. The two images are flipped by changing the helicity from LCP to RCP [Fig. 3(d)]. By scanning the "QR code" with a smart phone, one can access our group website (Ref. [27]).

Figure 4 shows the experimental and simulation results upon illumination of incident light with various polarization states. Two separate holographic images [see Figs. 4(a) and 4(e)] are observed when the device is illuminated by a circularly polarized light beam (RCP or LCP). The holographic images will overlap when a light beam with elliptical polarization impinges on the device since any polarized light beam can be decomposed into two beams with opposite circular polarization states. The rise and fall of intensities of two overlapping images is determined by the ellipticity of polarized light, which is controlled by the angle between the fast axis of the quarter wave plate and the transmission axis of the polarizer. The intensities of two overlapping images are the same [see Fig. 4(c)] for the linearly polarized light since it contains a LCP light beam and a RCP light beam with the same components. The intensity of the "QR code" dominates [see Fig. 4(d)] for the right-hand elliptically polarized light. Finally, two separate images are obtained again, but they are swapped and flipped [see Fig. 4(e)] compared to those in Fig. 4(a). Good agreement is seen between the experimental measurements and the simulation results.

We further evaluate the second functionality of the developed device—an arbitrary polarization profile for the hidden image. The schematic of the experimental setup to characterize the hidden image is shown in Fig. 5(a). Although the two bright laser beams in Fig. 3(c) along the vertical direction can be seen clearly, their detailed information (e.g., intensity, polarization) cannot be directly obtained due to the smaller beam size. In order to visualize the image on a charge-coupled device (CCD) camera, an objective with magnification of 10× is adopted to

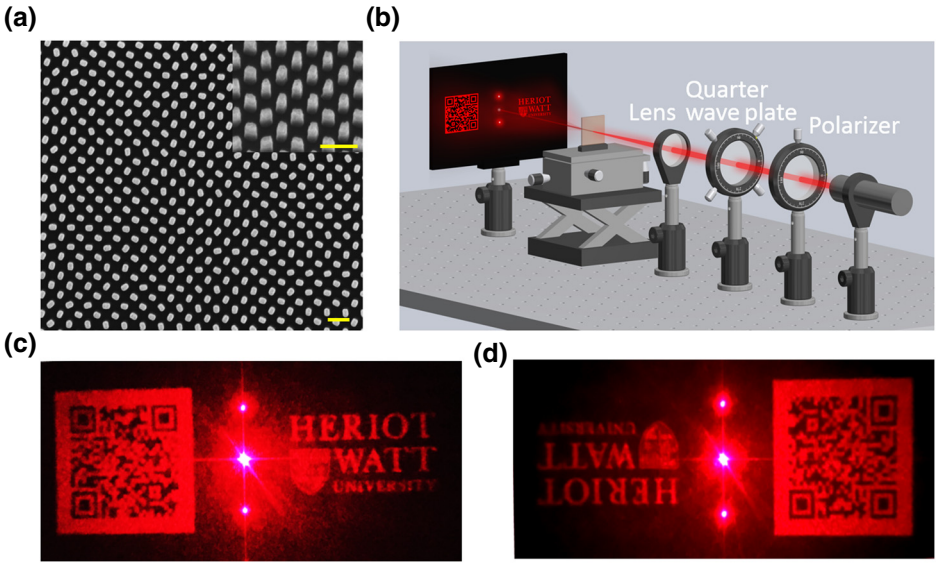

FIG. 3. SEM image of the fabricated device and experimental results. (a) SEM image of the fabricated sample. The scale bar is 500 μm. (b) Schematic of the experimental setup for the characterization of the designed hologram. The reconstructed holographic images consist of a "QR code" and a "University logo" upon the illumination of (c) LCP light and (d) RCP light.

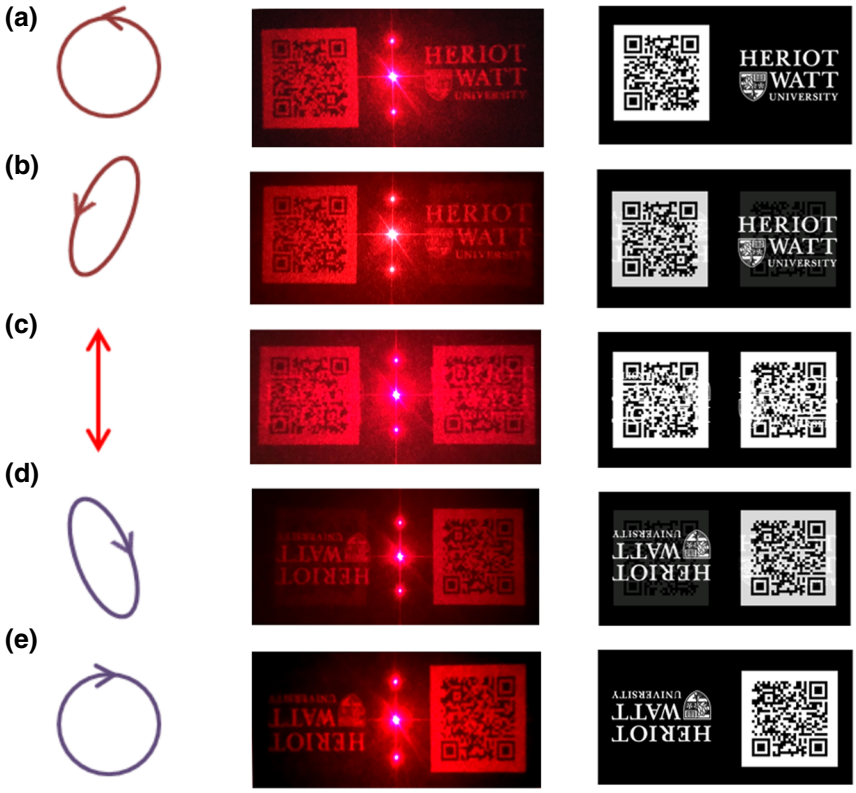

FIG. 4. Experimental results and simulation results of holographic images versus the polarization states of the incident light at 650 nm. The polarization states of the incident light are chosen to be (a) LCP, (b) left-hand elliptically polarized, (c) linearly polarized, (d) right-hand elliptically polarized, and (e) RCP. The figures in the middle column and right column represent the experimental results and the corresponding simulation results, respectively.

expand the image. To evaluate the generated polarization profile for the hidden image, the device is rotated by 90°, enabling the two vector beams along the horizontal direction and facilitating characterization. The transmission axes of the polarizer and the analyzer are along the horizontal and vertical directions, respectively. Detailed information about the experimental setup is provided in Sec. 2 of the Supplemental Material [26]. No image is obtained without the analyzer due to the uniform intensity distribution [see Fig. 5(b)]. The hidden image is decoded correctly only when the transmission axis of the analyzer is along the vertical direction [Fig. 5(c) left]. A plane wave with uniform intensity is used for the simulation, whereas a collimated laser beam with Gaussian profile is used in

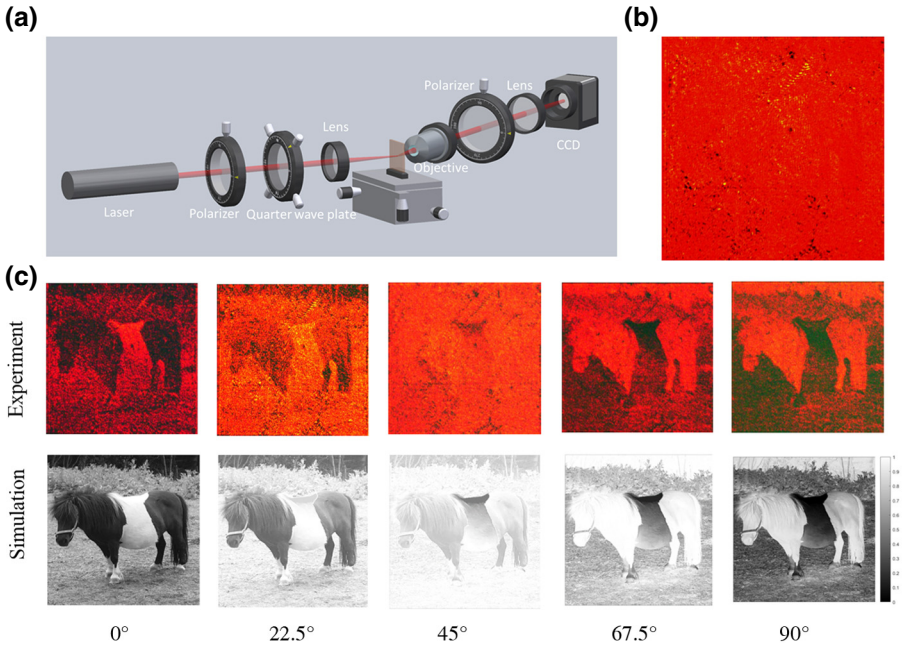

FIG. 5. Schematic of the experimental setup and characterization of the hidden image. (a) Experimental setup for the decoding of the hidden images. (b) Measured result without analyser. (c) The dependence of experimental results on the rotation angles of the transmission axis of the analyzer away from the vertical direction. The incident light is linearly polarized along the horizontal direction.

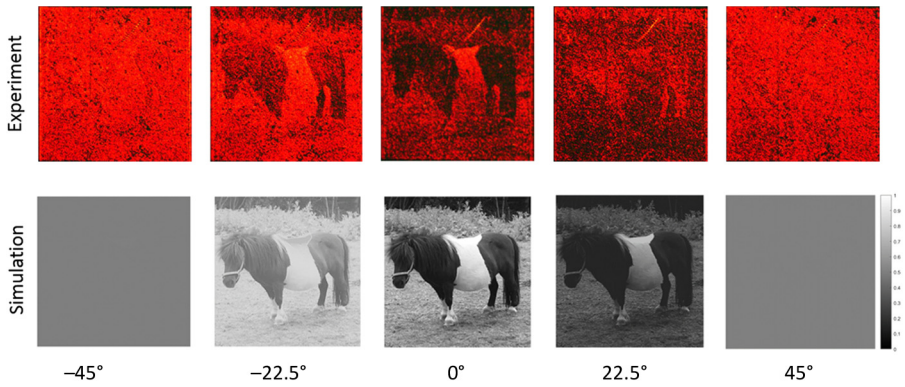

FIG. 6. The dependence of experimental results on polarization states of the incident light. The angles between the transmission axis of a linear polarizer (fixed along the horizontal direction) and the fast axis of the QWP are set at −45°, −22.5°, 0°, 22.5°, and 45°, respectively.

the experiment. The dependence of simulation and experimental results on the direction of the transmission axis of the analyzer are provided in Fig. 5(c), indicating that the transmission axis of the analyzer plays an important role in the decryption process. The two images for the analyzer with orthogonal transmission axes (0° and 90°) are complementary grayscale images, that is, the brightest area becomes the darkest area and vice versa. Under the illumination of the incident light with various polarization states, the numerically calculated and experimentally observed images are provided in Fig. 6. Despite the fact that the metadevice can work for elliptical polarization, the image quality is deteriorated.

IV. DISCUSSION

The uniqueness of this multichannel device is the integration of totally different functionalities on a single device by the independent control of phase and polarization profiles. Holography is one of the most attractive approaches for reconstructing optical images. As the largest part of the hologram market, security holograms have been used widely in our daily lives (e.g., passports, credit cards, quality products). However, despite tremendous advances in the fundamental principles of optical holography, traditional security holograms are not secure any more since they can be easily forged. Industry is always looking for holograms with unique properties that are not easy to design and are difficult to copy. Unlike the multiplexed metasurface holograms that can generate multiple holographic images by controlling polarization states of the incident light and the detection light, our device is the marriage between a helicity multiplexed hologram and a spatially variant polarization profile (not hologram), which can increase the level of anticounterfeiting. The holographic images are designed based on the Gerchberg-Saxton algorithm, while the hidden image is directly imprinted into the polarization distribution of the light beam based on Malus' law. By controlling the helicity of the incident light, the helicity multiplexed holographic images can be reconstructed directly without the need of additional optical elements to control the polarization state of the detection light, which is necessary for the polarization multiplexed hologram in Ref. [16]. However, an analyzer is necessary for the acquisition of the hidden image's intensity profile since the spatially varying polarization profile of the modulated light beam has a uniform intensity profile. To reveal the detailed information in the hidden image, an objective is needed due to the limited size of the device. Different from the vectorial hologram [24], the generated polarization profile is not a holographic image. The invention of this alternative device will possess a unique advantage over traditional security holograms due to the combination of image-switchable functionality and image encryption in the laser beam. In the terms of fabrication, the proposed hologram is much more tolerant to fabrication errors such as misalignment and etch-depth deviation since the designed geometric metasurface only needs a single lithography step. The conversion efficiency is defined as the ratio between the optical power with desired polarization rotation and the transmitted power. To perform optical measurement of the conversion efficiency, we fabricate a metasurface consisting of nanopillars with uniform orientations. The experimental setup is shown in Fig. S3 (in Sec. 3 of the Supplemental Material [26]). The simulated and experimental conversion efficiency [28] are shown in Fig. S4. In addition to the ultrathin nature and compactness, this multifunctional metadevice can provide entirely different functions that are very challenging or impossible to achieve with traditional optical components even with the highest quality.

V. CONCLUSION

Optical metasurfaces are capable of generating optical fields with inhomogeneous spatial distribution in terms of phase and polarization, providing a powerful tool to develop a multichannel device with unusual functionalities. We experimentally demonstrate a metasurface device that can realize image-switchable holograms and spatial polarization manipulation in different channels. The metadevice consists of amorphous silicon nanopillars with the same geometry and spatially variant orientations. The feasibility study of the multichannel device based on the

independent control of phase and polarization renders this technique very attractive for compact optical devices with high density of functionalities for anticounterfeiting and encryption. The security level of this approach can be further enhanced by using polarization-sensitive color holograms and encrypting a color image.

ACKNOWLEDGMENTS

This work is supported by Engineering and Physical Sciences Research Council of the United Kingdom (Grant No. EP/P029892/1). F.D. acknowledges the National Natural Science Foundation of China (Grants No. 61875042 and No. 11627803), the Youth Innovation Promotion Association CAS (Grant No. 2015030), CAS Key Technology Talent Program, and Key Research Program of Frontier Sciences, CAS (Grant No. QYZDB-SSW-SYS031). G.Z. acknowledges the National Natural Science Foundation of China (Grants No. 11774273 and No. 11574240).

X.C. and C.Z. initiated the idea. C. Z., X. Z., G.Z., and X.C. conducted the numerical simulations. F.D., L.X., and Z.S. fabricated the samples. C.Z., Y.I., and X.Z. performed the measurements. All the authors discussed and analyzed the results. X.C. and W.C. supervised the project. All the authors prepared the manuscript.

C.Z. and F.D. contributed equally to this work.

[1] N. Yu, P. Genevet, M. A. Kats, F. Aieta, J. P. Tetienne, F. Capasso, and Z. Gaburro, Light propagation with phase discontinuities: Generalized laws of reflection and refraction, Science **334**, 333 (2011).

[2] X. Ni, N. K. Emani, A. V. Kildishev, A. Boltasseva, and V. M. Shalaev, Broadband light bending with plasmonic nanoantenas, Science **335**, 427 (2012).

[3] X. Chen, L. Huang, H. Mühlenbernd, G. Li, B. Bai, Q. Tan, G. Jin, C. Qiu, S. Zhang, and T. Zentgraf, Dual-polarity plasmonic metalens for visible light, Nat. Commun. **3**, 1198 (2012).

[4] J. Lin, M. J. P. B. Mueller, Q. Wang, G. Yuan, N. Antoniou, X. Yuan, and F. Capasso, Polarization-controlled tunable directional coupling of surface plasmon polaritons, Science **340**, 331 (2013).

[5] M. Khorasaninejad, W. T. Chen, R. C. Devlin, J. Oh, A. Y. Zhu, and F. Capasso, Metalenses at visible wavelengths: Diffraction-limited focusing and subwavelength resolution imaging, Science **352**, 1190 (2016).

[6] L. Huang, X. Chen, H. Mühlenbernd, H. Zhang, S. Chen, B. Bai, Q. Tan, G. Jin, K.-W. Cheah, C.-W. Qiu, J. Li, T. Zentgraf, and S. Zhang, Three-dimensional optical holography using a plasmonic metasurface, Nat. Commun. **4**, 2808 (2013).

[7] G. Zheng, H. Muhlenbernd, M. Kenney, G. Li, T. Zentgraf, and S. Zhang, Metasurface holograms reaching 80% efficiency, Nat. Nanotechnol. **10**, 308 (2015).

[8] D. Wen, F. Yue, G. Li, G. Zheng, K. Chan, S. Chen, M. Chen, K. F. Li, P. W. H. Wong, K. W. Cheah, E. Y. B. Pun, S. Zhang, and X. Chen, Helicity multiplexed broadband metasurface holograms, Nat. Commun. **6**, 8241 (2015).

[9] X. Ni, A. V. Kildishev, and V. M. Shalaev, Metasurface holograms for visible light, Nat. Commun. **4**, 2807 (2013).

[10] Z. Li, Q. Dai, M. Q. Mehmood, G. Hu, B. Luk'yanchuk, J. Tao, C. Hao, I. Kim, H. Jeong, G. Zheng, S. Yu, A. Alù, J. Rho, and C.-W. Qiu, Full-space cloud of random points with a scrambling metasurface, Light Sci. Appl. **7**, 63 (2018).

[11] Z. Li, I. Kim, L. Zhang, M. Q. Mehmood, M. S. Anwar, M. Saleem, D. Lee, K. T. Nam, S. Zhang, B. Luk'yanchuk, Y. Wang, G. Zheng, J. Rho, and C.-W. Qiu, Dielectric meta-holograms enabled with dual magnetic resonances in visible light, ACS Nano **11**, 9382 (2017).

[12] X. Yin, Z. Ye, J. Rho, Y. Wang, and X. Zhang, Photonic spin Hall effect at metasurfaces, Science **339**, 1405 (2013).

[13] F. Yue, D. Wen, C. Zhang, B. D. Gerardot, W. Wang, S. Zhang, and X. Chen, Multichannel polarization-controllable superpositions of orbital angular momentum states, Adv. Mater. **29**, 1603838 (2017).

[14] Y. Chen, X. Yang, and J. Gao, Spin-controlled wavefront shaping with plasmonic chiral geometric metasurfaces, Adv. Opt. Mater. **6**, 1800646 (2018).

[15] G. Li, S. Zhang, and T. Zentgraf, Nonlinear photonic metasurfaces, Nat. Rev. Mater. **2**, 17010 (2017).

[16] R. Zhao, B. Sain, Q. Wei, C. Tang, X. Li, T. Weiss, L. Huang, Y. Wang, and T. Zentgraf, Multichannel vectorial holographic display and encryption, Light Sci. Appl. **7**, 95 (2018).

[17] A. Arbabi, Y. Horie, M. Bagheri, and A. Faraon, Dielectric metasurfaces for complete control of phase and polarization with subwavelength spatial resolution and high transmission, Nat. Nanotechnol. **10**, 937 (2015).

[18] Z. Zhang, D. Wen, C. Zhang, M. Chen, W. Wang, S. Chen, and X. Chen, Multifunctional light sword metasurface lens, ACS Photonics **5**, 1794 (2018).

[19] F. Yue, C. Zhang, X.-F. Zang, D. Wen, B. D. Gerardot, S. Zhang, and X. Chen, High-resolution grayscale image hidden in a laser beam, Light Sci. Appl. **7**, 17129 (2018).

[20] F. Dong and W. Chu, Multichannel-independent information encoding with optical metasurfaces, Adv. Mater. 1804921 (2018).

[21] W. T. Chen, K. Y. Yang, C. M. Wang, Y. W. Huang, G. Sun, I.-D. Chiang, C. Y. Liao, W.-L. Hsu, H. T. Lin, S. Sun, L. Zhou, A. Q. Liu, and D. P. Tsai, High-efficiency broadband meta-hologram with polarization-controlled dual images, Nano Lett. **14**, 225 (2014).

[22] Y. W. Huang, W. T. Chen, W. Y. Tsai, P. C. Wu, C. M. Wang, G. Sun, and D. P. Tsai, Aluminum plasmonic multicolor meta-hologram, Nano Lett. **15**, 3122 (2015).

[23] B. Wang, F. Dong, Q.-T. Li, D. Yang, C. Sun, J. Chen, Z. Song, L. Xu, W. Chu, Y.-F. Xiao, Q. Gong, and Y. Li, Visible-frequency dielectric metasurfaces for multiwavelength achromatic and highly dispersive holograms, Nano Lett. **16**, 5235 (2016).

[24] Z. L. Deng, J. Deng, X. Zhuang, S. Wang, K. Li, Y. Wang, Y. Chi, X. Ye, J. Xu, G. P. Wang, R. Zhao, X. Wang,

Y. Cao, X. Cheng, G. Li, and X. Li, Diatomic metasurface for vectorial holography, Nano Lett. **18**, 2885 (2018).

[25] R. W. Gerchberg and W. O. Saxton, A practical algorithm for the determination of phase from image and diffraction plane pictures, Optik **35**, 237 (1972).

[26] See Supplemental Material at http://link.aps.org/supplemental/10.1103/PhysRevApplied.12.034028 for further details of off-axis design of the metasurface, characterization of the hidden image, and conversion efficiency measurement.

[27] (http://nanophotonicslab.eps.hw.ac.uk/).

[28] X. Zang, F. Dong, F. Yue, C. Zhang, L. Xu, Z. Song, M. Chen, P. Y. Chen, G. S. Buller, Y. Zhu, S. Zhuang, S. Zhang, W. Chu, and X. Chen, Polarization encoded color image embedded in a dielectric metasurface, Adv. Mater. **30**, 1707499 (2018).